Steel and Composite Structures, *Vol. 32, No. 1* (*2019*) *141-156*
DOI: https://doi.org/10.12989/scs.2019.32.1.141

Behaviour of large fabricated stainless steel beam-to-tubular column joints with extended endplates

Jia Wang*, Brian Uy [a] and Dongxu Li [b]

School of Civil Engineering, *The University of Sydney*, *Sydney*, *NSW 2006*, *Australia*

(*Received April 5, 2019, Revised May 29, 2019, Accepted May 29, 2019*)

Abstract. This paper presents the flexural behaviour of stainless steel beam-to-tubular column joints with extended endplates subjected to static loading. Moment-rotation relationships were investigated numerically by using Abaqus software with geometric and material nonlinearity considered. The prediction of damages among components was achieved through ductile damage models, and the influence of initial geometric imperfections and residual stresses was evaluated in large fabricated stainless steel joints involving hollow columns and concrete-filled columns. Parametric analysis was subsequently conducted to assess critical factors that could affect the flexural performance significantly in terms of the initial stiffness and moment resistance. A comparison between codes of practice and numerical results was thereafter made, and design recommendations were proposed for further applications. Results suggest that the finite element model can predict the structural behaviour reasonably well with the component damage consistent with test outcomes. Initial geometric imperfections and residual stresses are shown to have little effect on the moment-rotation responses. A series of parameters that can influence the joint behaviour remarkably include the strain-hardening exponents, stainless steel strength, diameter of bolts, thickness of endplates, position of bolts, section of beams and columns. AS/NZS 2327 is more reliable to predict the joint performance regarding the initial stiffness and moment capacity compared to EN 1993-1-8.

Keywords: stainless steel; beam-to-column joint; tubular column; concrete-filled column; residual stress

1. Introduction

Stainless steel has gained growing popularity in engineering practice during the last few decades owing to its various benefits such as high ductility, significant strain hardening, better corrosion and impact resistance, and relatively low maintenance expenses in the whole life cycle (Han *et al*. 2019, Hasan *et al*. 2017 and Yousuf *et al*. 2014). These preferable benefits contribute to a wide range of applications of stainless steel as the primary structural material in building and bridge construction (Baddoo 2008 and Paul *et al*. 2017). Currently, a vast majority of stainless steel structures are based on a cold-formed manufacturing process. However, large fabricated stainless steel structures are expected to achieve a wider application in mega projects and complicated structural forms by virtual of its flexible fabrication. Although the high initial cost, resulting from the chemical composition of nickel, temporarily limits an extensive use as an alternative to carbon steel, it is advisable to promote academic research on the stainless steel structures in order to have a comprehensive understanding of the structural behaviour, and to propose robust design guidance.

Considerable previous research has been carried out to investigate the performance of stainless steel beams, columns and connections (Dai and Lam 2010, Lee *et al*. 2014, Kim and Lim 2013, Kiymaz and Seckin 2014 and Averseng *et al*. 2017). Arrayago and Real (2016) and Gkantou *et al*. (2019) performed experimental studies on simply supported and continuous beams to investigate the flexural behaviour in terms of the cross-section slenderness limits. Comparisons between test results and design codes were thereafter made to assess the adequacy of current specifications for stainless steel. Tondini *et al*. (2013), Huang and Young (2014), Jandera and Machacek (2014) and Tokgoz (2015) investigated the performance of stainless steel columns under fire conditions, eccentric loading and biaxial loading experimentally and numerically. Residual stress distribution patterns were explored to evaluate the influence on the column behaviour. Research results were compared with design provisions throughout the world contributing to the improvement of design guidance. Lui *et al*. 2014, Zhao *et al*. 2016 and Lopes *et al*. 2019 discussed the structural performance of stainless steel beam-columns subjected to various loading conditions. By means of experimental programmes and numerical analysis, three types of stainless steel including austenitic, ferritic and duplex were considered respectively to look into the varied behaviour. Cai and Young (2018) reviewed a wide range of literature regarding stainless steel bolted connections at ambient and elevated temperature. A suggested design bearing resistance factor was compared to the current design codes and proved to be applicable to various

*Corresponding author, Ph.D.,
E-mail: jia.wang@sydney.edu.au
[a] Professor, E-mail: brian.uy@sydney.edu.au
[b] Ph.D., E-mail: dongxu.li@sydnedy.edu.au

ISSN: 1229-9367 (Print), 1598-6233 (Online)

stainless steel materials. In addition, the shear response of stainless steel bolted connections loaded at varied stain rates was also assessed by Cai and Young (2019). The design resistance was compared with design standards from Australia, Europe and USA indicating that Eurocodes were more reliable to predict the results.

It is clear that most studies mentioned above focused on commonly used structures, while beam-to-column joints involving stainless steel were less discussed. Although Tao *et al*. (2017) executed a spectrum of experimental programmes on blind bolted connections to concrete-filled stainless steel columns, only the tubular columns were fabricated by stainless steel. The remaining steel components were made of carbon steel instead. It is noted that Elflah *et al*. (2018a, b and 2019) elaborated the moment-rotation relationship of stainless steel beam-to-column joints through experiments and finite element modelling, but the analysis did not incorporate the effect of residual stress which commonly existed in welded structures. In addition, the joints with tubular columns only involved flush endplates which were quite different from extended endplates. As a result, it is necessary to extend the research to the behaviour of large fabricated stainless steel structures.

This paper investigates the flexural performance of large fabricated stainless steel beam-to-column joints with extended endplates and hollow or concrete-filled columns. Finite element models (FEM) were initially developed based on experimental programmes published previously, and the corresponding test results were selected to validate the accuracy of FEM. Another fabricated stainless steel beam-to-column joint models were then set up taking residual stresses and initial geometric imperfections into consideration. Parametric analysis was subsequently employed to discuss factors affecting joint behaviour broadly. Lastly, the numerical models were assessed by design specifications with the metrics of initial stiffness and moment capacity.

2. Numerical modelling

Three-dimensional finite element models of beam-to-column joints were developed by using Abaqus software (2016) considering geometric and material nonlinearity. Exterior columns and extended endplates were selected to investigate the joint performance under single-sided bending moments. Three types of joint models were initially developed and calibrated based on the literature from Elflah *et al*. (2018a), Korol *et al*. (1993), Wang and Chen (2012). The specific structural configurations are outlined in Table 1. The benchmark model consisting of stainless steel hollow or concrete-filled columns, I-section beams, extended endplates and blind bolts was then created to perform further investigation.

2.1 Development of FEM

All typical components of joints were generated by solid elements including beams, columns, endplates and bolts. Since welds between endplates and beams exhibited sufficient strength and stiffness, and no fracture was reported in the literature as well, they were not developed explicitly in Abaqus. Instead, the welds were replaced by the tie restraint which connected endplates and beams firmly. The identical method was also used for welds between beams and stiffeners. Apart from that, modelling of bolts was simplified by ignoring threads and integrating bolt nuts, washers and bolt shanks into single parts.

Explicit solver algorithm was adopted to eliminate the issue of convergence difficulty and conveniently achieve material damage simulation as well. Appropriate step time for each analysis needs to be determined carefully since it represents the elapsed real time where a small value can induce impact effects due to the high speed of loading. Conversely, a large value leads to redundant computation costs. To avoid the impact effects which were not in line with quasi-static requirements, energy outputs were monitored including the internal energy and kinetic energy. Results were accounted reliable given that the kinetic energy took up less than 2% of internal energy (Elflah *et al*. 2018b).

As for the contact interaction, general contact algorithm was complied which was preferable due to its simplicity and convenience. Both penalty friction formulation with the coefficient of 0.3 and hard contact strategy were deployed to define the interaction property. Translations on the top and bottom of columns were constrained while the out-of-plane translation of beams was prevented from twisting deformations. Vertical loads were applied to the end of beams by using the displacement control strategy with a smooth step. It is noteworthy that the model from Wang and Chen (2012) incorporated axial loads for columns. The identical conditions were applied, and it can be achieved by deploying surface pressures on the top of columns.

Stress-strain relationships of stainless steel were obtained from each test results which are summarised in Table 2. Stress-strain relationship of stainless steel is remarkably different from carbon steel due to a lack of the yield plateau in stainless steel. Typical information for all stainless steel components was abstracted from Elflah *et al*. (2018a), and the stress-strain curves were derived based on the Ramberg-Osgood model (1943) and Mirambell's model (Mirambell and Real 2000).

$$\varepsilon = \frac{\sigma}{E_0} + 0.002(\frac{\sigma}{\sigma_{0.2}})^{n_{0,0.2}} \tag{1}$$

$$n_{0,0.2} = \frac{\ln(20)}{\ln(\sigma_{0.2}) - \ln(\sigma_{0.1})}, \sigma < \sigma_{0.2} \tag{2}$$

$$\varepsilon = \frac{\sigma - \sigma_{0.2}}{E_{0.2}} + (\varepsilon_u - \varepsilon_{0.2} - \frac{\sigma_u - \sigma_{0.2}}{E_{0.2}}) \times (\frac{\sigma - \sigma_{0.2}}{\sigma_u - \sigma_{0.2}})^{n_{0.2,u}} + \varepsilon_{0.2}, \sigma > \sigma_{0.2} \tag{3}$$

where $n_{0,0.2}$ and $n_{0.2,u}$ are exponents related to strain hardening.

True stress and plastic strain are required to be imported into Abaqus, which can be converted from nominal stress and strain shown as below

Table 1 Summary of joint specimen

Reference	Specimen	Column section $h_c \times b_{fc} \times t_{fc} \times t_{wc} \times H$ (mm)	Beam section $h_b \times b_{fb} \times t_{fb} \times t_{wb} \times L$ (mm)	Endplate $D \times B \times t_p$ (mm)	Bolts	Axial load (kN)
Elflah *et al*. (2018a)	EEP	240×120×12×10×1500 (I section)	240×120×12×10×1500 (I section)	330×120×8	M16	0
Korol *et al*. (1993)	S4	254×254×9.53×9.53×1200 (Square)	349×127×8.5×5.8×2400 (I section)	550×230×19	M20	0
Wang and Chen (2012)	MES1	200×200×10×10×1625 (Square)	300×150×10×6×1700 (I section)	540×200×12	M20	2204

*Note: h_c, b_{fc}, t_{fc}, t_{wc} and H is the depth, flange width, flange thickness, web thickness and height of columns, respectively; h_b, b_{fb}, t_{fb}, t_{wb} and L is the depth, flange width, flange thickness, web thickness and length of beams, respectively; D, B and tp is the depth, width and thickness of endplate, respectively

Table 2 Material properties of components

Reference	Component	Young's modulus E_0 (MPa)	Yield strength σ_{ys} / $\sigma_{0.2}$ (MPa)	Ultimate strength σ_{us}	Elongation ε_f (%)	$n_{0,0.2}$	$n_{0.2,u}$	Compressive cube strength σ_{uc}
Elflah *et al*. (2018a)	Flange	196,500	306	630	66	5.2	2.37	-
	Web	205,700	320	651	65	6.7	2.41	-
	Endplate	198,000	343	655	54	12.2	2.5	-
	Bolt	191,500	617	805	12	17.24	3.68	-
Korol *et al*. (1993)	Beam flange	210,000	300	440	-	-	-	-
	Beam web	210,000	350	440	-	-	-	-
	Endplate	210,000	300	440	-	-	-	-
	Column	210,000	350	440	-	-	-	-
	Bolt	210,000	508	750	-	-	-	-
Wang and Chen (2012)	Beam flange	187,000	349.3	492	16.5	-	-	-
	Beam web	216,000	312.5	508.3	17.4	-	-	-
	Endplate	198,000	323.3	436.7	31.0	-	-	-
	Column	201,000	328.1	490.6	21.7	-	-	-
	Bolt	200,000	900	1000	12.5	-	-	-
	Concrete	31,878	-	-	-	-	-	44.3
Author	Beam flange	188,800	328.5	659.8	55.5	6.9	-	-
	Beam web	188,600	312.6	695.7	60.6	5.8	-	-
	Endplate	198,000	343	655	54	12.2	2.5	-
	Column	188,600	312.6	695.7	60.6	5.8	-	-
	Bolt (M20)	191,500	617	805	12	17.24	3.68	-
	Concrete	31,878					-	44.3

$$\sigma_{true} = \sigma_{nom}(1+\varepsilon_{nom}) \tag{4}$$

$$\varepsilon_{true}^{pl} = \ln(1+\varepsilon_{nom}) - \sigma_{true}/E_0 \tag{5}$$

Test results are collected in Table 2. The component fracture was captured in most tests resulting in a sharp or gradual drop in the moment-rotation curves. As such, the material damage was considered by deploying ductile damage models to simulate component fractures. The simulating strategy was proposed by Pavlović *et al*. (2013), and has been demonstrated by Wang *et al*. (2018b) that the method was reliable to predict the structural behaviour of joints. In particular, the bolt fracture is critical to the joint performance since its relatively low ductility contributes to the insufficient rotational capacity of joints. Therefore, the accurate prediction of bolt damage is desired. In this case, the finite element modelling of a single bolt under axial tension was firstly conducted, followed by the calibration with experimental results to determine parameters of ductile damage models in Abaqus. These parameters involved the fracture stain and plastic displacement from the onset of damage to fracture. The confined concrete property which was recommended by Shams and Saadeghvaziri (1999) and Mursi and Uy (2003) was adopted. Young's modulus and

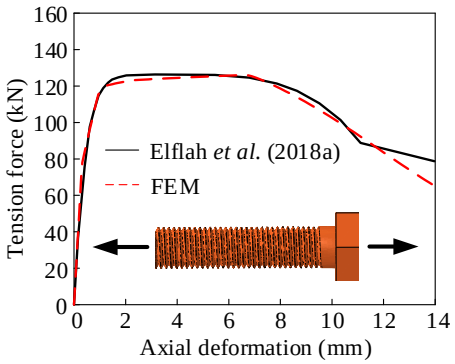

Fig. 1 Load-displacement curve of bolt in tension

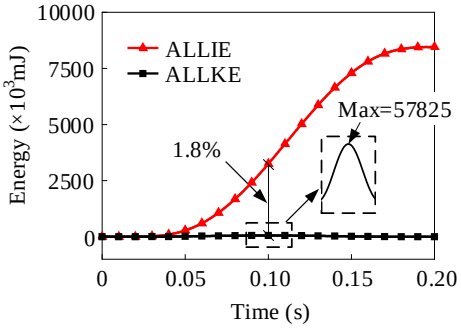

Fig. 2 Comparison between strain energy and kinetic energy

compressive strength of concrete are collected in Table 2.

2.2 Model validation

As mentioned above, the bolt damage has significant influences on the reliability of simulation. The load-displacement curves of bolts under axial tension were compared between numerical and experimental outcomes shown in Fig. 1. The comparison indicates a good consistency proving that the adopted parameters of ductile damage models can be further used to predict the joint behaviour. Numerical results of joint specimens were validated with experimental data reported by Elflah *et al.* (2018a), Korol *et al.* (1993) and Wang and Chen (2012). Fig. 2 displays the energy outputs including the strain energy and kinetic energy for the explicit algorithm obtained from Elflah's model. The maximum value of kinetic energy only accounts for 1.8% of the strain energy at the corresponding position, which means the loading speed is acceptable for quasi-static analysis without impact effects induced.

Fig. 3 describes failure modes and deformations of beam-to-column joints with extended endplates at the end of loading based on experimental and numerical outputs. It can be seen that the finite element model can predict the flexural response reasonably well. Both structural specimens experienced large rotations where endplates undertook extensive bending moments. With respect to the stainless steel joint in Fig. 3(a), stainless steel bolts at the

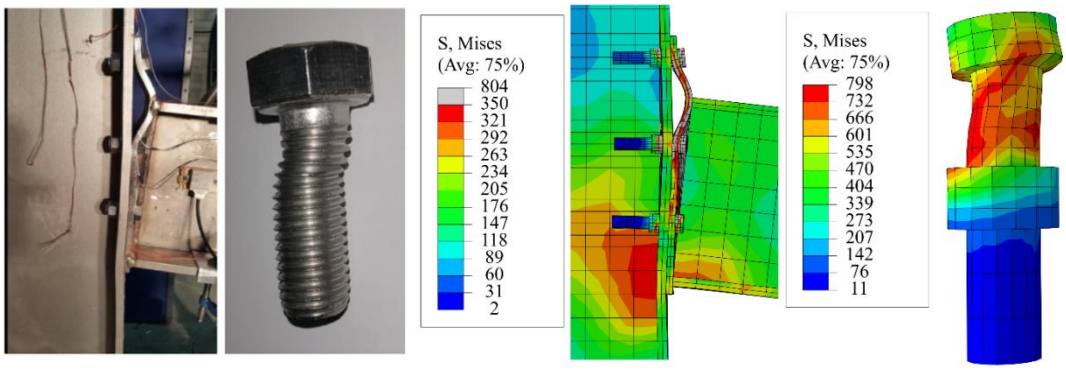

(a) Steel joint (Elflah *et al.* 2018a)

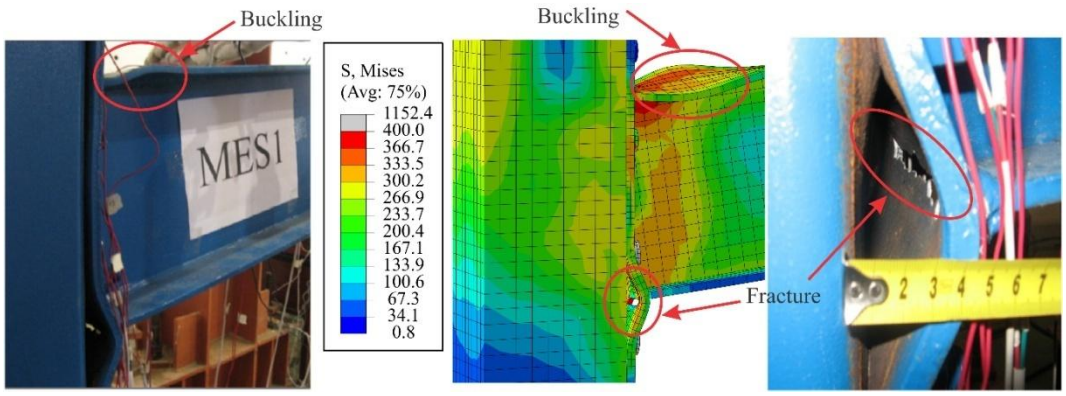

(b) Joint with concrete-filled column (Wang and Chen 2012)

Fig. 3 Comparison between experimental and numerical results

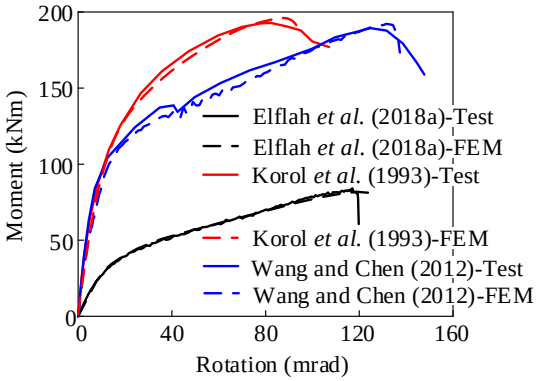

Fig. 4 Moment-rotation curve validationc

top two rows close to the beam flange in tension deformed remarkably due to large tension and prying forces. The significant deformations of the endplate indicated that the high ductility of stainless steel rendered structures performing well even under large strains. As for the carbon steel joint in Fig. 3(b), the endplate in tension region encountered fracture under the maximum load, which was captured by the finite element model. The difference further highlighted that stainless steel is more ductile than carbon steel. It is noteworthy that the specimen in Fig. 3(b) was placed upside down and was subjected to a reverse load.

Moment-rotation curves of all models are depicted in Fig. 4 incorporating a comparison between the test and numerical results. The comparison suggests that the numerical method has a good agreement with experimental programmes. Moreover, the numerical method is able to capture the component failure that results in a sharp or gradual drop in the moment resistance. Therefore, based on the comparison in terms of failure modes and moment-rotation relationship, it can be concluded that the numerical method is reliable to predict the flexural performance of stainless steel beam-to-column joints with extended endplates and hollow or concrete-filled columns.

2.3 Modelling of large fabricated stainless steel joints

The validated FEM was further extended to investigate the flexural behaviour of large fabricated stainless steel joints. Two types of beam-to-column joints were included, namely joints with hollow columns and concrete-filled columns. Additionally, welding-induced residual stresses and initial geometric imperfection were introduced into FEM in this section. The aim is to investigate the effect of residual stresses on the fabricated stainless steel members that are distinct from cold-formed structures. Meanwhile, initial geometric imperfections render large stainless steel structures more sensitive to local buckling behaviour in theory. Overall, the procedure of FEM was similar as mentioned in Section 2.1 except that columns and beams were replaced by welded stainless steel components referring to Yuan *et al*. (2014). Geometric details are described in Fig. 5, and material properties of the adopted beams and columns are summarised in Table 2.

The pretension of bolts was achieved by deploying negative temperature to bolt shanks to generate tensile stress due to the constraint of endplate and column walls. By trial and error, the temperature of -190℃ can generate 75 kN tensile force for bolts. The related expansion factor of stainless steel was taken as 1.65×10^{-5}. Apart from that, axial compressive loads were applied on the top of columns to simulate loading conditions in a multi-storey structure. The ratio of axial loads to ultimate compressive capacity of columns was set as $\omega = N_c/N_u$. Tao *et al*. (2017) suggested the value ranged from 0.58 to 0.7, and thus 0.6 was initially determined for the original models. The ultimate compressive capacity of hollow column was defined by EN 1993-1-1 (2005) which incorporated buckling resistance, while the capacity of concrete-filled columns can be estimated based on EN 1994-1-1 (2004) as listed below

$$\text{Hollow column: } N_u = \frac{\chi A \sigma_y}{\gamma_{M1}} \tag{6}$$

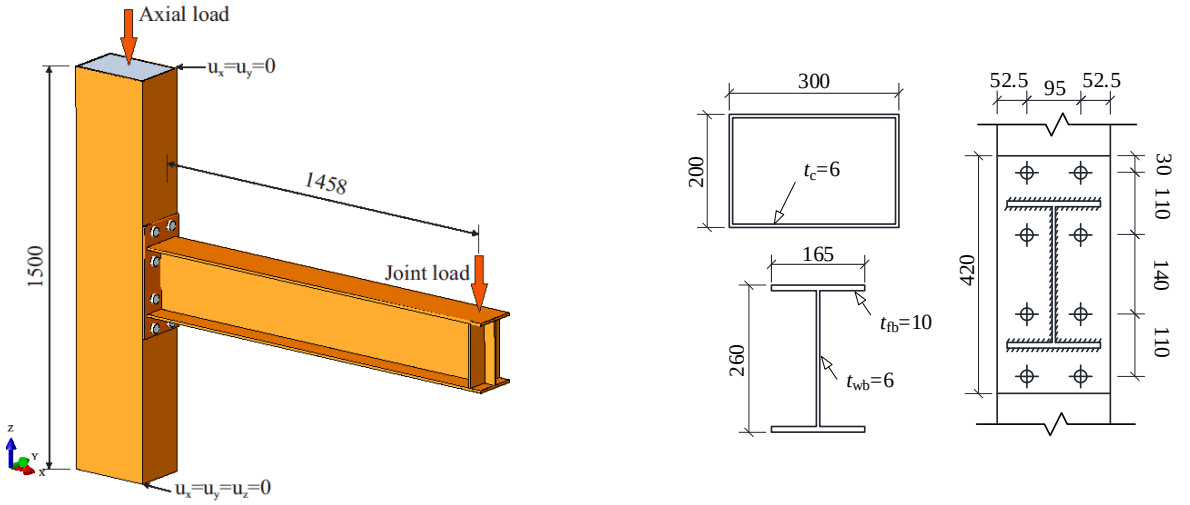

Fig. 5 Geometry details of stainless steel joints (Unit: mm)

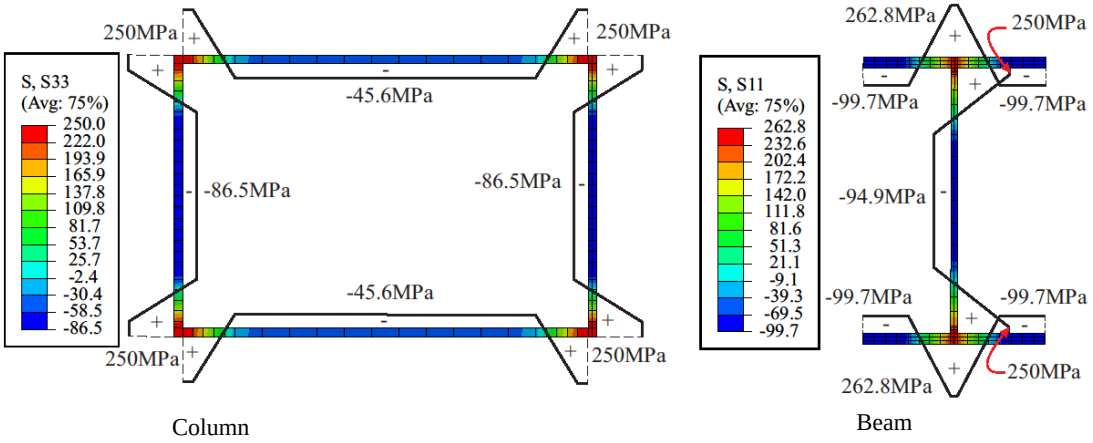

Column Beam

Fig. 6 Distribution of residual stress in FE models

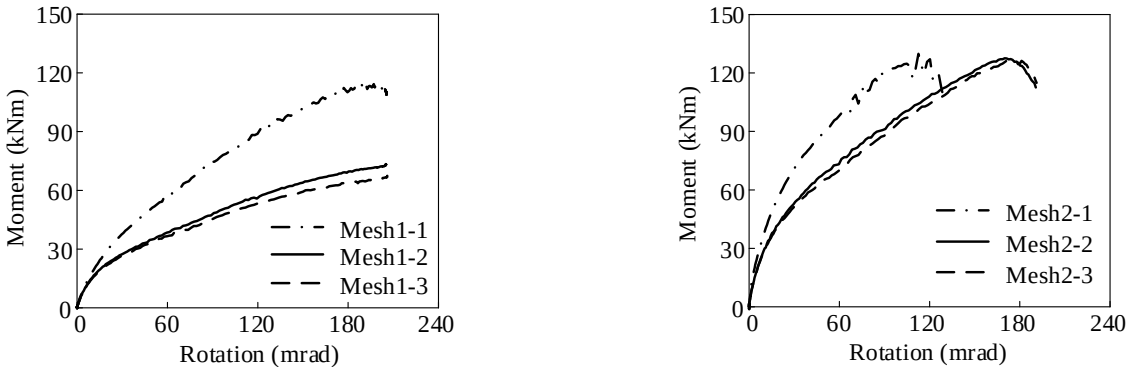

(a) Joints with hollow columns (b) Joints with concrete-filled columns

Fig. 7 Mesh convergence

$$\chi = \frac{1}{\Phi + \sqrt{\Phi^2 - \bar{\lambda}^2}} \leq 1.0 \tag{7}$$

$$\Phi = 0.5[1 + \alpha(\bar{\lambda} - 0.2) + \bar{\lambda}^2] \tag{8}$$

$$\bar{\lambda} = \sqrt{\frac{A\sigma_y}{N_{cr}}} \tag{9}$$

$$\text{Concrete-filled column: } N_u = A_s\sigma_{sy} + A_c\sigma_{uc} \tag{10}$$

where α is an imperfection factor; N_{cr} is the elastic critical force for the relevant buckling mode based on the gross cross-sectional properties.

Fig. 6 depicts the welding residual stress distribution obtained from experimental results reported by Yuan *et al.* (2014) regarding box-section and I-section members. The distribution patterns were deployed to finite element models through defining predefined filed stress for beams and columns in which only normal stresses perpendicular to cross sections was taken into account. For simplicity, residual stresses on welding regions between endplates and beams were ignored. The initial geometric imperfection effect in FE models was simulated by updating geometrical

Table 3 Element size details (Unit: mm)

Model no.	Column	Beam	Endplate	Bolt	Concrete
Mesh1-1	30	30	15	8	-
Mesh1-2	20	20	10	4	-
Mesh1-3	15	15	8	3	-
Mesh2-1	30	30	15	8	35
Mesh2-2	20	20	10	4	25
Mesh2-3	15	15	8	3	20

information of all nodes obtained from linear buckling analysis. The desired buckling modes with multi-orders were initially determined by buckling analysis, and the original FE models were subsequently modified by these buckling modes incorporated with amplification factors.

The first-order mode was typically critical, and more large-order modes can be accumulated readily to consider complicated imperfections. The related amplification factors were defined in accordance with recommendations of design provisions. EN 1993-1-1 (2005) suggests the ratio of imperfections to member length to be 1/200 along the major axis and 1/150 along the minor axis for welded I-sections. In addition, EN 1993-1-5 (2006) recommends that imperfections should be taken as the minimum value of

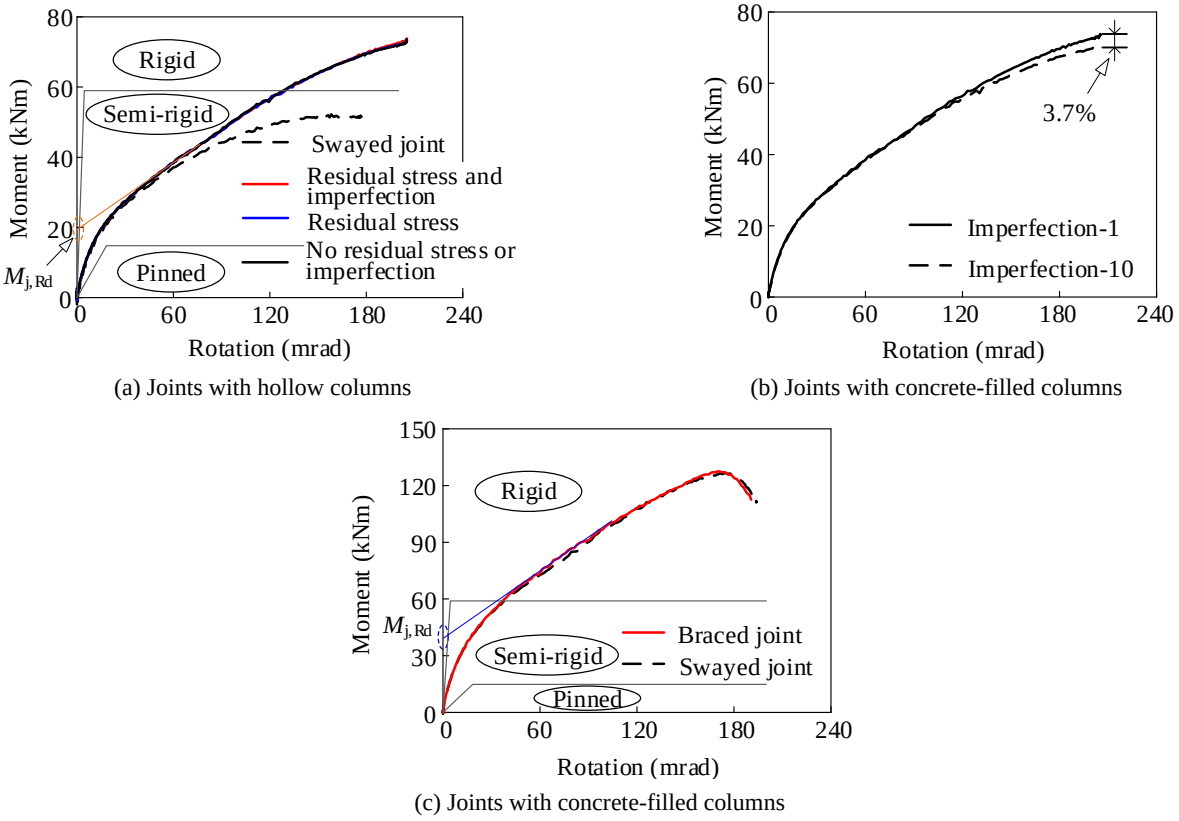

(a) Joints with hollow columns

(b) Joints with concrete-filled columns

(c) Joints with concrete-filled columns

Fig. 8 Moment-rotation curve

depth or length of plates divided by 200. Regarding models in this paper, two recommendations were combined by accumulating multi-order buckling modes.

2.3.1 Mesh convergence analysis

Mesh convergence analysis was carried out in order to determine the optimum element dimensions which can not only secure the accuracy but also save computing time. Accordingly, various numerical models were set up with varied mesh sizes. Element size details are outlined in Table 3 and the results are compared in Fig. 7 for both types of joints.

The comparison suggested that the numerical results tended to increase in terms of the initial stiffness and moment resistance if element sizes rose to some extent. Since damage parameters were related to the element size, it is clear that the joint with the hollow column (Mesh1-1) and concrete-filled column (Mesh2-1) suffered damages in advance which led to inaccurate results due to the significant dimensional deviation. Conversely, when smaller element sizes were used, the moment-rotation curves were shown to remain stable. However, the finer mesh cannot contribute to more precise results but increased computing cost. As such, the preferred element sizes in Mesh1-2 and Mesh2-2 were adopted for further analysis as a result of accuracy and low analysis time.

2.3.2 Results and discussion

Fig. 8 describes the moment-rotation curves of joints with hollow columns and concrete-filled columns. Based on the boundary conditions of columns, the joints were divided into braced or swayed structures. Those with the horizontal translations of columns constrained were accounted braced structures, whereas the counterparts were regarded as swayed structures. It can be seen that the flexural behaviour of joints with hollow columns is remarkably different between these two types of structures, but the difference in the joints with concrete-filled columns is small. It is due to the fact that the flexural stiffness of hollow columns is lower than that of concrete-filled columns. Concerning the joints with hollow columns, various models were developed involving residual stresses and initial geometric imperfections. It is found that both factors have limited effects on the behaviour of beam-to-column joints in braced systems. It is to be expected since buckling behaviour is normally correlated to compressive members, while the current structures are subjected to bending moments. As a result, the discrepancy remains insignificant even if the imperfection amplification factor increases to ten times as shown in Fig. 8(b). Meanwhile, the flexural members are not sensitive to residual stresses. As such, no residual stresses or initial imperfections are considered anymore for simplicity.

It is noted that both joints are classified as semi-rigid joints which exhibits sufficient ductility. The initial stiffness of joints with concrete-filled columns approaches 5794 kNm/rad that is higher than the joints with hollow columns. The discrepancy is owing to the contribution of concrete filled in columns which induces an increase in the stiffness of column web in shear and tension and column flange in bending. Moreover, the ultimate moment resistance of joints with concrete-filled columns is larger than that of joints

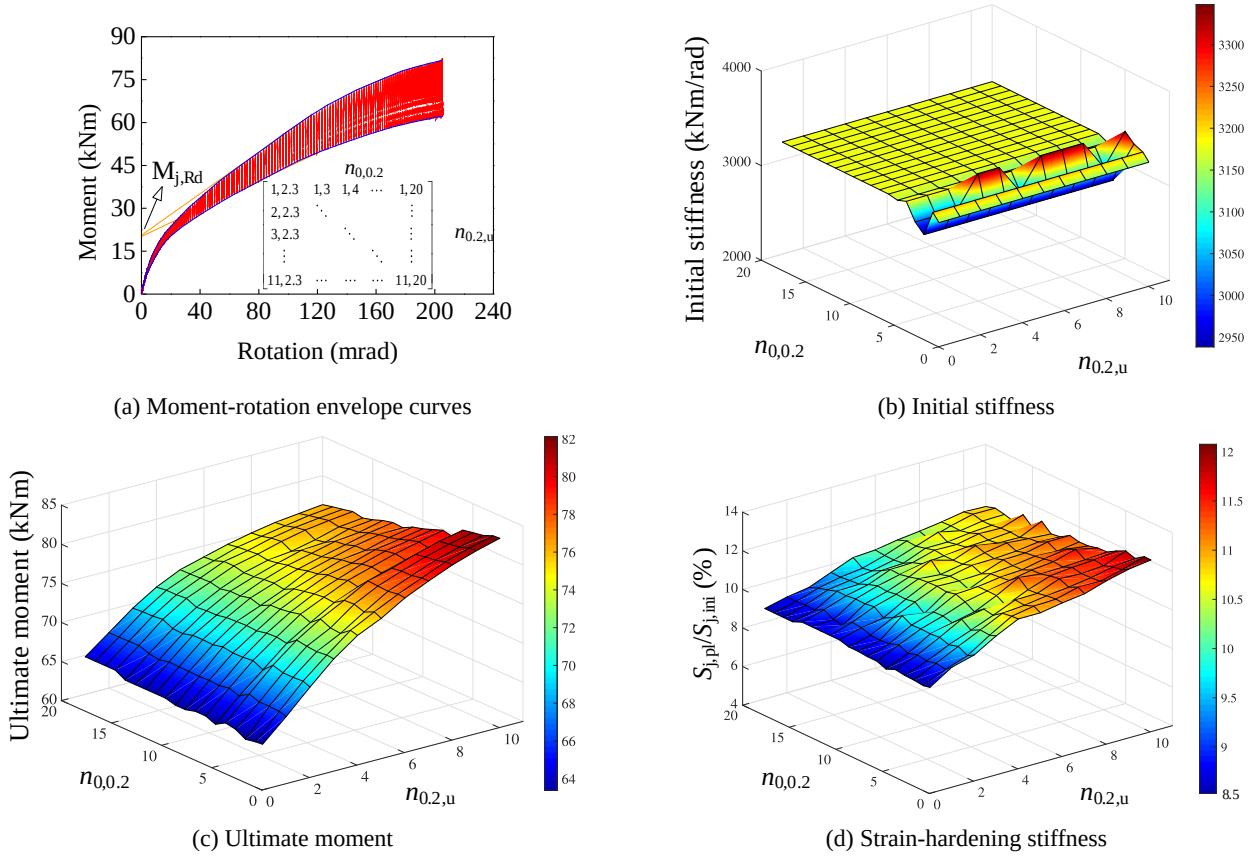

(a) Moment-rotation envelope curves

(b) Initial stiffness

(c) Ultimate moment

(d) Strain-hardening stiffness

Fig. 9 Summary of results caused by strain hardening exponents

with hollow column significantly. Plastic moment resistance $M_{j,Rd}$, defined as moment capacity by EN 1993-1-8 (2010), can be determined according to Jaspart (1991). Namely, it is the intersection between secant modulus and *y*-axis representing the moment resistance of certain component experiencing yielding stress. Figs. 8(a) and (c) indicate that the plastic moment resistance of joints with hollow and concrete-filled columns is 26.1 kN·m and 36.5 kN·m, respectively.

3. Parametric analysis

Further analysis was performed by varying parameters that influenced the structural behaviour remarkably. These parameters consisted of the strain-hardening exponents, strength of stainless steel, strength of concrete, axial load ratios, diameter of bolts, thickness of endplates, position of bolts, section of beams and columns. The specific configurations are summarised in Table 4. Flexural performance of both steel joints (SJ) and joints with concrete-filled columns (CJ) was evaluated respectively to classify different responses.

3.1 Effects of strain-hardening exponents ($n_{0,0.2}$, $n_{0.2,u}$)

As discussed above, the stress-strain curve of stainless steel is related to two strain-hardening exponents, $n_{0,0.2}$, $n_{0.2,u}$,which are determined experimentally. The value of $n_{0,0.2}$ can range from 3 to 17 and the value of $n_{0.2,u}$ varies from 1.75 to 6 in different types of stainless steel according to published literature (Mirambell and Real 2000, Rasmussen 2003, Gardner and Nethercot 2004, Ashraf *et al*. 2008, Real *et al*. 2014, Arrayago *et al*. 2015 and Elflah *et al*. 2019). Their effects on the moment-rotation behaviour of joints were hence investigated aiming to find out envelope curves reflecting the initial stiffness, moment capacity and strain-hardening stiffness. Accordingly, a total of 209 models with $n_{0,0.2}$ increasing from 2.3 to 20 and $n_{0.2,u}$ rising from 1 to 11 were developed for steel joints and the corresponding moment-rotation curves are plotted in Fig. 9(a). It is shown that the plastic performance is largely influenced by the strain-hardening exponents, and the moment resistances corresponding to the same rotation vary largely. However, the moment capacity $M_{j,Rd}$ remains stable, indicating that the value only depends on yield strength rather than strain-hardening exponents.

Figs. 9(b)-(d) further illustrate the varied structural behaviour of joints under an array of exponents. It is found that the initial stiffness of all models cannot be affected remarkably despite some ignorable fluctuations. The phenomenon is to be expected since the initial stiffness is related to the Young's modulus of material and geometry. On the other hand, the significant fluctuations in the ultimate moment resistance and strain-hardening stiffness are observed. Regarding the ultimate moment resistance, the influence of strain-hardening exponent $n_{0.2,u}$ is larger than $n_{0,0.2}$. As a result, the parameter $n_{0.2,u}$ should be

Table 4 Parameters for parametric study

Joint	Model no.	$\sigma_{0.2}$ (MPa)	σ_u (MPa)	f_c (MPa)	Load ratio ω	D_b (mm)	t_{ep} (mm)	m_x (mm)	e_x (mm)	m (mm)	e (mm)	B_{ep} (mm)	H (mm)	h_1 (mm)	h_2 (mm)
	EN 1.4301	**328.5**	**659.8**	44.3	0.6	20	8	40	30	34.5	52.5	200	420	50	140
	EN 1.4462	**574.8**	**775.0**	44.3	0.6	20	8	40	30	34.5	52.5	200	420	50	140
	EN 1.4658	**800**	**1000**	44.3	0.6	20	8	40	30	34.5	52.5	200	420	50	140
	C30	328.5	659.8	**28**	0.6	20	8	40	30	34.5	52.5	200	420	50	140
	C40	328.5	659.8	**44.3**	0.6	20	8	40	30	34.5	52.5	200	420	50	140
	C60	328.5	659.8	**60**	0.6	20	8	40	30	34.5	52.5	200	420	50	140
	LR-0	328.5	659.8	44.3	**0**	20	8	40	30	34.5	52.5	200	420	50	140
	LR-0.6	328.5	659.8	44.3	**0.6**	20	8	40	30	34.5	52.5	200	420	50	140
	LR-1.0	328.5	659.8	44.3	**1.0**	20	8	40	30	34.5	52.5	200	420	50	140
	M16	328.5	659.8	44.3	0.6	**16**	8	40	30	34.5	52.5	200	420	50	140
	M20	328.5	659.8	44.3	0.6	**20**	8	40	30	34.5	52.5	200	420	50	140
	M24	328.5	659.8	44.3	0.6	**24**	8	40	30	34.5	52.5	200	420	50	140
	ET8	328.5	659.8	44.3	0.6	20	**8**	40	30	34.5	52.5	200	420	50	140
	ET12	328.5	659.8	44.3	0.6	20	**12**	40	30	34.5	52.5	200	420	50	140
SJ/CJ	ET16	328.5	659.8	44.3	0.6	20	**16**	40	30	34.5	52.5	200	420	50	140
	ET20	328.5	659.8	44.3	0.6	20	**20**	40	30	34.5	52.5	200	420	50	140
	m-24.5	328.5	659.8	44.3	0.6	20	8	**40**	**30**	**24.5**	**62.5**	200	420	50	140
	m-34.5	328.5	659.8	44.3	0.6	20	8	**40**	**30**	**34.5**	**52.5**	200	420	50	140
	m-44.5	328.5	659.8	44.3	0.6	20	8	**40**	**30**	**44.5**	**42.5**	200	420	50	140
	mx-25	328.5	659.8	44.3	0.6	20	8	**25**	**45**	**34.5**	**52.5**	200	420	50	140
	mx-15	328.5	659.8	44.3	0.6	20	8	**15**	**55**	**34.5**	**52.5**	200	420	50	140
	I-150	328.5	659.8	44.3	0.6	20	8	40	30	34.5	**52.5**	**200**	**290**	**40**	**50**
	I-252	328.5	659.8	44.3	0.6	20	8	40	30	34.5	**75**	**245**	**412**	**50**	**140**
	I-260	328.5	659.8	44.3	0.6	20	8	40	30	34.5	**52.5**	**200**	**420**	**50**	**140**
	I-372	328.5	659.8	44.3	0.6	20	8	40	30	34.5	**75.5**	**246**	**532**	**50**	**260**
	R300-200	328.5	659.8	44.3	0.6	20	8	40	30	34.5	52.5	200	420	50	140
	R150-200	328.5	659.8	44.3	0.6	20	8	40	30	34.5	52.5	200	420	50	140
	R160-160	328.5	659.8	44.3	0.6	20	8	40	30	34.5	52.5	200	420	50	140
	R300-300	328.5	659.8	44.3	0.6	20	8	40	30	34.5	52.5	200	420	50	140

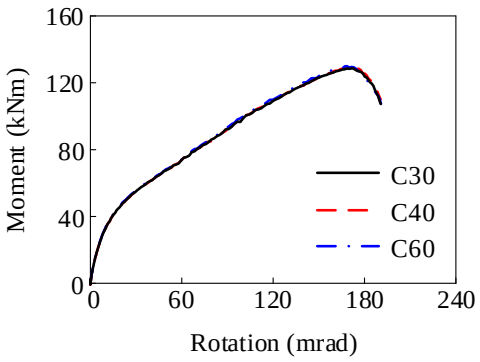

Fig. 11 Strength of concrete

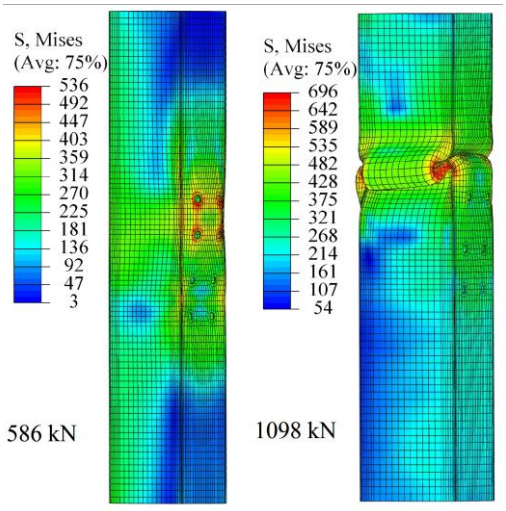

Fig. 12 Deformation of columns

determined with cautions such that an empirical expression is not appropriate. A similar conclusion can be drawn for the strain-hardening stiffness since the ratios of strain-

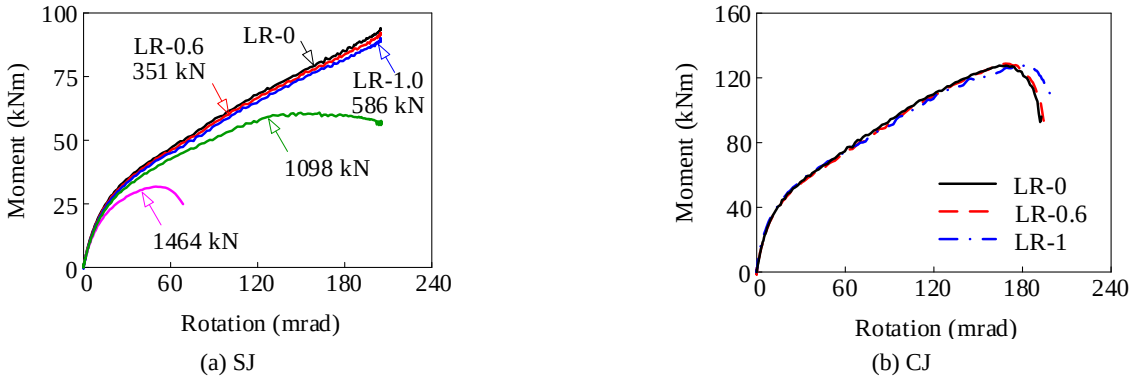

(a) SJ (b) CJ

Fig. 13 Axial load ratios

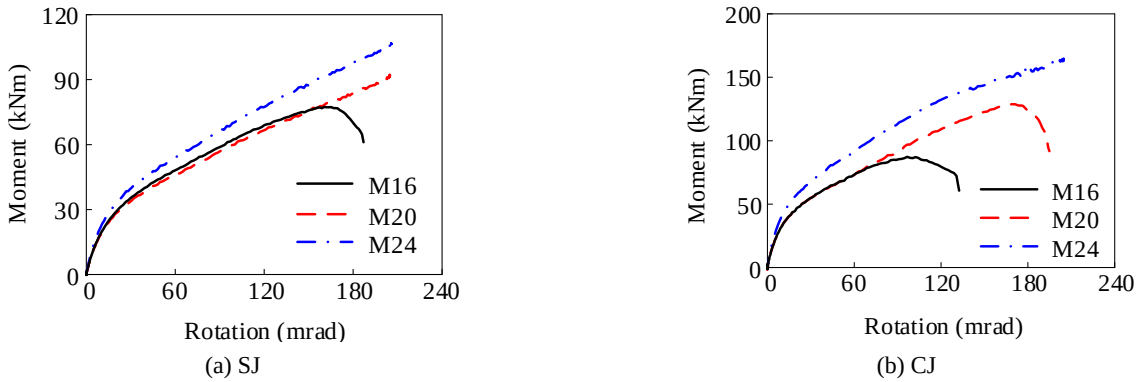

(a) SJ (b) CJ

Fig. 14 Diameter of bolts

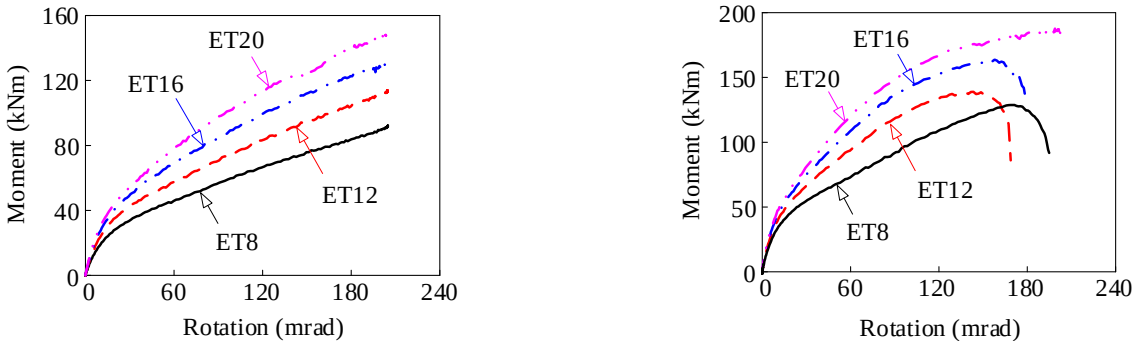

(a) SJ (b) CJ

Fig. 15 Thickness of endplates

hardening stiffness to initial stiffness fluctuate between 8.5% and 12%.

3.2 Effects of strength of stainless steel and concrete

Three types of stainless steel with different strength were employed by BS EN 10088-1 (2014) shown in Fig. 10. EN 1.4301 and EN 1.4462 were applied to all steel components except for bolts while EN 1.4658 was only used for bolts. It can be seen that the moment resistance corresponding to the same rotation increases significantly for steel joints if high strength of stainless steel EN 1.4462 is used. However, the improvement is neutralised in joints with concrete-filled columns since bolts are damaged in advance. In addition, there is a limited improvement of performance if bolts with higher strength are adopted despite that it contributes to a higher rotational capacity. As for the concrete strength, no difference between the moment-rotation behaviour is observed in Fig. 11 due to the fact that the role of concrete filled in columns is to enhance the flexural stiffness of joints.

3.3 Effects of axial load ratios

Fig. 13 indicates the moment-rotation responses of steel joints and joints with concrete-filled columns under various axial load ratios of compressive load to compressive

capacity of columns. Regarding steel joints, the compressive capacity with a buckling resistance threshold considered was initially adopted. Results suggest that different load ratios have small effects on flexural behaviour. The compressive capacity was then increased to the cross-section capacity (N_s). When it comes to 60% of N_s (1098 kN), it is noted that the moment resistance deteriorates significantly. If the axial load rises to 80% of N_s (1464 kN), the steel joints fail to undertake bending moments functionally. Fig. 12 compares the deformation of steel columns under two types of axial loads. It demonstrates that columns experienced buckling prior to joint failures under a higher compressive load. However, infilled concrete can avoid buckling sufficiently such that axial load ratios are found to have less effects on joints. Instead, the joints with concrete-filled columns encountered bolt damages in the end.

3.4 Effects of diameter of bolts

Three commonly used diameters of bolts were deployed to predict the moment-rotation curves of joints which are described in Fig. 14. It is found that the joints in SJ and CJ using M16 and M20 exhibit similar performance before failures. M20 bolts facilitate higher rotational capacity owing to higher moment resistance. M24 bolts are able to improve the joint behaviour further but the improvement is not considerable. As a result, M20 bolts are recommended in design as a practical and sufficient component.

3.5 Effects of endplate thickness

As shown in Fig. 15, the flexural performance of both forms of joints can be improved apparently by increasing the thickness of endplates from 8 mm to 20 mm in terms of the initial stiffness and moment resistance. The results are to be expected since the two mechanical metrics are related to the endplate in bending that dominates the flexural response. It is noted that endplates with larger thickness are recommended to improve the joint behaviour due to the use of more ductile stainless steel compared to carbon steel.

3.6 Effects of position of bolts

According to EN 1993-1-8 (2010), the initial stiffness and plastic moment resistance are dependent on the dimensions m, m_x, e, or e_x which are explained in Fig. 16. In this case, numerical analysis was carried out to estimate the effects of bolt positions, and the results are collected in Fig. 18. It is observed that the joint behaviour can be improved by locating bolts in vertical line far away from beam webs, namely increasing the value of m. The observation is different from provisions in EN 1993-1-8 which suggest the behaviour should be enhanced by placing bolts in vertical line closer to beam webs because the stiffness of endplate in bending can be increased. The contradiction attributes to the fact that tubular columns are used in this research instead of open-section columns. In this case, the flexural stiffness of column in tension can be increased more remarkably than endplate in bending by putting bolts in vertical line away from beam webs. In addition, moving bolts in row towards beam flanges can achieve improvements as well, namely decreasing the value of m_x, and it is more effective than the former method.

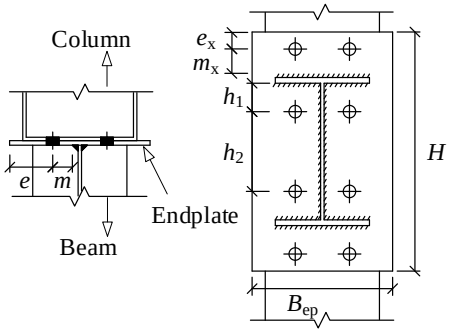

Fig. 16 Definition of parameters related to position of bolts

3.7 Effects of section of beams and columns

Four types of beam sections were applied involving non-compact (I-150 and I-260) and slender (I-252 and I-372) profiles based on AS 4100 (1998) to investigate the flexural response. Figs. 16 and 17 specify all parameters related to beam sections. Endplates were adjusted along with beams while other components remained identical. It can be seen from Fig. 19 that the initial stiffness and ultimate moment resistance rise with an increase in the height of beams. As for I-252 and I-260, the joints exhibit the similar performance due to the approximative height of beams despite different section slenderness. It reveals that the performance of semi-rigid joints is not dominated by the beam moment capacity.

Likewise, four kinds of column sections were utilised including compact (R160-160), non-compact (R150-200) and slender (R300-200 and R300-300) profiles. Simultaneously, no other components were changed in this study. The results shown in Fig. 20 indicate that the joints

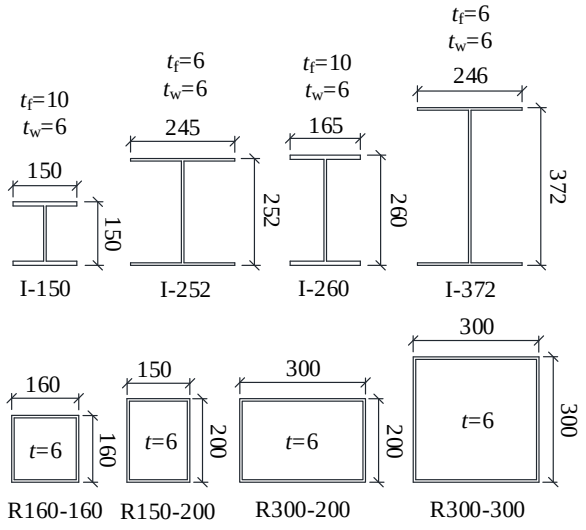

Fig. 17 Definitions of parameters related to beam and column sections (Unit: mm)

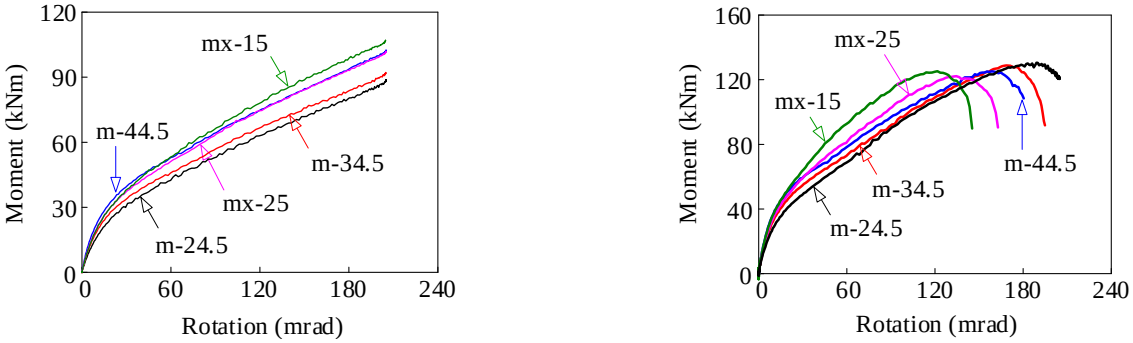

(a) SJ (b) CJ

Fig. 18 Position of bolts

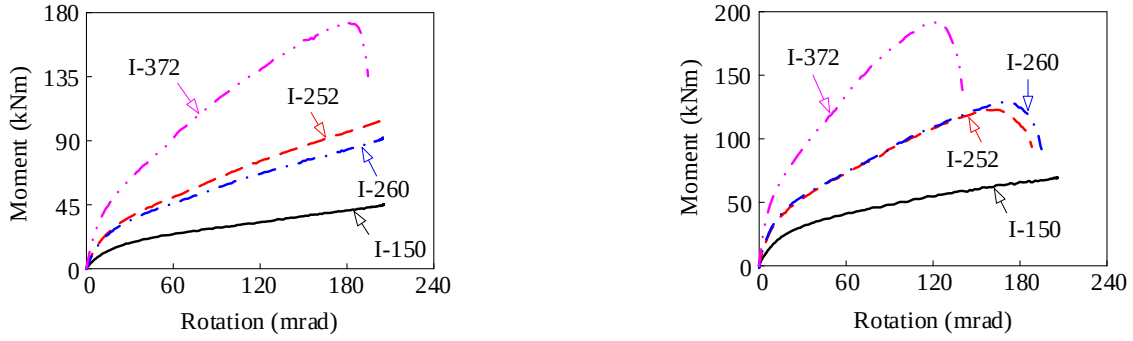

(a) SJ (b) CJ

Fig. 19 Section of beams

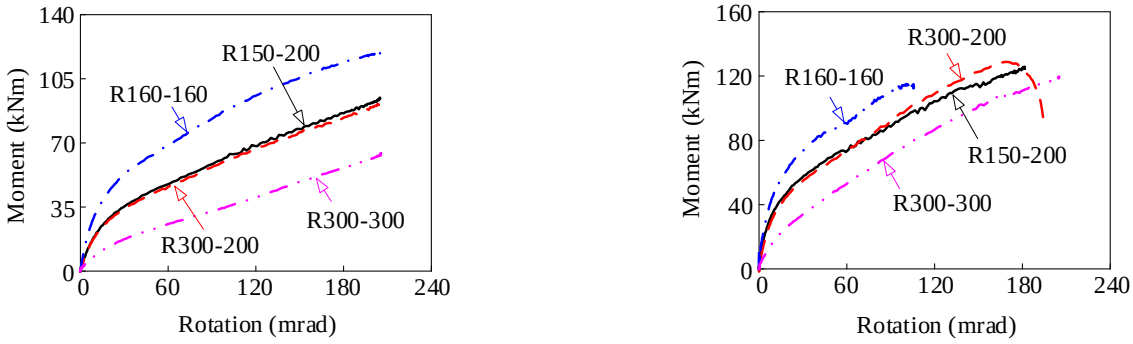

(a) SJ (b) CJ

Fig. 20 Section of columns

were strengthened by decreasing the width of column wall adjacent to endplates in terms of the initial stiffness and moment capacity. It is noted that the duplicate performance has been achieved by R150-200 and R300-200 which belong to different types of section slenderness. As such, it can be also concluded that the performance of semi-rigid joints is not governed by the column moment capacity. Besides, the side wall width of column has little contributions to the joint performance compared with the wall attached to endplates. However, columns with high sidewall width are preferred to provide sufficient flexural rigidity, because the column in R160-160 experienced significant deflections so that the rotation of joints declined.

4. Assessment of codes of practice and design recommendations

EN 1993-1-8 (2010) and AS/NZS 2327 (2017) both clarify design provisions for beam-to-column joints with carbon steel. The former mainly involves joints with unstiffened or stiffened open-section columns while the later extends to hollow-section columns. Both codes of practice were employed to compare with the finite element results obtained from the parametric analysis in terms of the initial stiffness and moment capacity. The summary is outlined in Table 5 and Fig. 21 including all discussed parameters except for concrete strength and axial load ratios

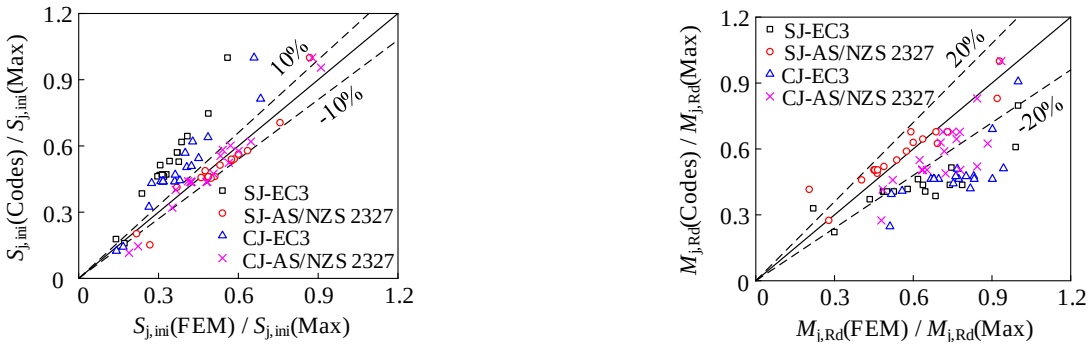

(a) Initial stiffness (b) Moment capacity

Fig. 21 Comparison between FEM and design codes

Table 5 Result comparison between FEM and design provisions

Joint	Model No.	Initial stiffness $S_{j,ini}$ (kN·m/rad)					Moment capacity $M_{j,Rd}$ (kN·m)					$S_{j,pl}$ / $S_{j,ini}$ (%)
		$S_{j,ini}$ (FEM)	$S_{j,ini}$ (EC3)	$S_{j,ini}$ (AS/NZS 2327)	EC3/ FEM	AS/NZS 2327/ FEM	$M_{j,Rd}$ (FEM)	$M_{j,Rd}$ (EC3)	$M_{j,Rd}$ (AS/NZS 2327)	EC3/ FEM	AS/NZS 2327/ FEM	
SJ (CJ)	EN 1.4301	3412 (5794)	5085 (8030)	3219 (5996)	1.49 (1.39)	0.94 (1.03)	26.1 (36.5)	21.7 (24.9)	29.0 (29.0)	0.83 (0.68)	1.11 (0.79)	9.9 (10.5)
	EN 1.4462	3311 (6619)	5085 (8030)	3219 (5996)	1.54 (1.21)	0.97 (0.91)	53.4 (53.8)	42.6 (48.8)	57.5 (57.5)	0.80 (0.91)	1.08 (1.07)	10.6 (12.3)
	EN 1.4658	3412 (6599)	5085 (8030)	3219 (5996)	1.49 (1.22)	0.94 (0.91)	25.9 (37.5)	21.7 (24.9)	29.0 (29.0)	0.84 (0.66)	1.12 (0.77)	10.3 (9.5)
	M16	3220 (5008)	5028 (7884)	3197 (5508)	1.56 (1.57)	0.99 (1.10)	26.6 (41.6)	21.7 (24.9)	28.1 (28.1)	0.82 (0.60)	1.06 (0.68)	11.0 (10.5)
	M20	3412 (5794)	5085 (8030)	3219 (5996)	1.49 (1.39)	0.94 (1.03)	26.1 (36.5)	21.7 (24.9)	29.0 (29.0)	0.83 (0.68)	1.11 (0.79)	9.9 (10.5)
	M24	3582 (6958)	5116 (8112)	3232 (6515)	1.43 (1.17)	0.90 (0.94)	28.1 (48.5)	21.7 (24.9)	29.9 (29.9)	0.77 (0.51)	1.06 (0.62)	11.9 (10.3)
	ET8	3412 (5794)	5085 (8030)	3219 (5996)	1.49 (1.39)	0.94 (1.03)	26.1 (36.5)	21.7 (24.9)	29.0 (29.0)	0.83 (0.68)	1.11 (0.79)	9.9 (10.5)
	ET12	4032 (7317)	6199 (10397)	3736 (7624)	1.54 (1.42)	0.93 (1.04)	34.0 (41.0)	23.3 (25.6)	39.0 (39.0)	0.69 (0.62)	1.15 (0.95)	10.2 (12.1)
	ET16	4203 (7837)	6715 (11324)	3941 (8260)	1.60 (1.44)	0.94 (1.05)	39.5 (43.1)	23.3 (25.6)	39.0 (39.0)	0.59 (0.59)	0.99 (0.90)	11.9 (13.9)
	ET20	4443 (8883)	7001 (11685)	4046 (8511)	1.58 (1.32)	0.91 (0.96)	42.0 (44.7)	23.3 (25.6)	39.0 (39.0)	0.55 (0.57)	0.93 (0.87)	13.5 (14.1)
	m-24.5	2584 (4830)	4175 (5916)	2885 (4400)	1.62 (1.22)	1.12 (0.91)	23.2 (30.0)	19.8 (22.0)	26.4 (26.4)	0.85 (0.73)	1.14 (0.88)	12.8 (13.6)
	m-34.5	3412 (5794)	5085 (8030)	3219 (5996)	1.49 (1.39)	0.94 (1.03)	26.1 (36.5)	21.7 (24.9)	29.0 (29.0)	0.83 (0.68)	1.11 (0.79)	9.9 (10.5)
	m-44.5	4093 (7428)	5744 (9209)	3783 (7996)	1.40 (1.24)	0.92 (1.08)	33.0 (41.3)	24.7 (27.4)	33.9 (33.9)	0.75 (0.66)	1.03 (0.82)	8.4 (8.2)
	mx-25	3717 (7748)	5777 (9300)	3590 (7182)	1.55 (1.20)	0.97 (0.93)	34.5 (40.5)	21.7 (23.8)	36.2 (36.2)	0.63 (0.59)	1.05 (0.89)	8.9 (8.9)
	mx-15	4019 (8248)	6205 (9957)	3775 (7919)	1.54 (1.21)	0.94 (0.96)	36.6 (44.0)	20.6 (22.6)	37.1 (37.1)	0.56 (0.51)	1.01 (0.84)	8.7 (9.8)
	I-150	1873 (3061)	1729 (2605)	1064 (1994)	0.92 (0.85)	0.57 (0.65)	16.0 (27.5)	11.8 (13.3)	15.8 (15.8)	0.74 (0.48)	0.99 (0.57)	7.3 (7.4)
	I-252	3484 (5642)	5011 (8039)	3178 (6036)	1.44 (1.42)	0.91 (1.07)	30.9 (35.9)	22.3 (24.9)	31.6 (31.6)	0.72 (0.69)	1.02 (0.88)	10.6 (10.8)
	I-260	3412 (5794)	5085 (8030)	3219 (5996)	1.49 (1.39)	0.94 (1.03)	26.1 (36.5)	21.7 (24.9)	29.0 (29.0)	0.83 (0.68)	1.11 (0.79)	9.9 (10.5)

Table 5 Continued

Joint	Model No.	Initial stiffness $S_{j,ini}$ (kN·m/rad)					Moment capacity $M_{j,Rd}$ (kN·m)					$S_{j,pl}$ / $S_{j,ini}$ (%)
		$S_{j,ini}$ (FEM)	$S_{j,ini}$ (EC3)	$S_{j,ini}$ (AS/NZS 2327)	EC3/ FEM	AS/NZS 2327/ FEM	$M_{j,Rd}$ (FEM)	$M_{j,Rd}$ (EC3)	$M_{j,Rd}$ (AS/NZS 2327)	EC3/ FEM	AS/NZS 2327/ FEM	
SJ (CJ)	I-372	6079 (12054)	10870 (18283)	6999 (13730)	1.79 (1.52)	1.15 (1.14)	52.9 (48.5)	32.5 (37.1)	47.7 (47.7)	0.61 (0.76)	0.90 (0.98)	12.0 (11.8)
	R300-200	3412 (5794)	5085 (8030)	3219 (5996)	1.49 (1.39)	0.94 (1.03)	26.1 (36.5)	21.7 (24.9)	29.0 (29.0)	0.83 (0.68)	1.11 (0.79)	9.9 (10.5)
	R150-200	3329 (6629)	5573 (8579)	3413 (5996)	1.67 (1.29)	1.03 (0.90)	26.7 (44.8)	21.7 (24.9)	29.0 (29.0)	0.81 (0.56)	1.09 (0.65)	10.5 (7.7)
	R160-160	5296 (12504)	8117 (14876)	4938 (13112)	1.53 (1.19)	0.93 (1.05)	39.8 (50.8)	27.5 (27.5)	35.9 (35.9)	0.69 (0.54)	0.90 (0.71)	9.1 (6.1)
	R300-300	1524 (2598)	1932 (2276)	1414 (1588)	1.27 (0.88)	0.93 (0.61)	11.7 (27.8)	17.6 (21.2)	23.9 (23.9)	1.50 (0.76)	2.04 (0.86)	15.6 (18.8)
	Mean				1.50 (1.29)	0.94 (0.97)				0.78 (0.65)	1.10 (0.81)	10.5 (10.8)
	SD				0.16 (0.17)	0.10 (0.12)				0.18 (0.10)	0.21 (0.11)	

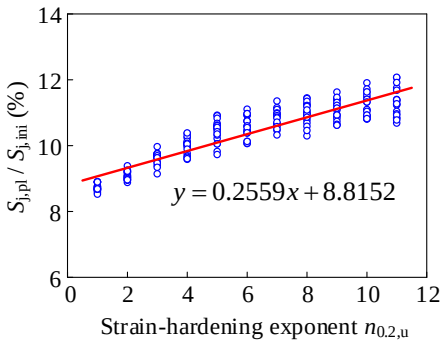

Fig. 22 Regression analysis of strain-hardening stiffness

which have little effects.

It is found that AS/NZS 2327 can provide more accurate predictions of initial stiffness for joints with hollow-section or concrete-filled columns than EN 1993-1-8. It attributes to the optimized algorithm with respect to the stiffness coefficient of column face in bending. The mean precision rate approaches 0.94 and 0.97 for both joints even though it underestimates the initial stiffness of specimen I-150. The reason can be that the beam height is such small that more than two rows of bolts tend to be subjected to tension. However, only two rows are considered in the assessment resulting in smaller stiffness. Regarding the moment capacity, AS/NZS 2327 still has a better agreement with the FEM results than EN 1993-1-8 despite that the tolerance scope (20%) is larger than that of the initial stiffness (10%) as shown in Fig. 21. It is noted that the moment capacity of joints with concrete-filled columns determined by EN 1993-1-8 is based on stiffened columns since the infilled concrete is regarded as stiffeners offering additional supports to prevent column faces from buckling. On the other hand, the moment capacity defined by AS/NZS 2327 remains constant between specimens SJ and CJ because it lacks supplementary explanations for concrete-filled columns. In a nutshell, AS/NZS 2327 is more reliable to predict the initial stiffness and moment capacity of joints with tubular columns.

Both design codes define the moment capacity on the basis of yield strength of materials resulting in over conservative predictions of stainless steel joint behaviour. As can be seen from the moment-rotation curves, the ultimate moment resistance exceeds moment capacity significantly reaching more than three times. The underestimation typically limits the application of stainless steel and impairs its advantages, leading to the waste of materials. As such, it is necessary to take the strain-hardening effects into account which can be quantised by strain-hardening stiffness, $S_{j,pl}$. Previous research by Wang *et al*. (2018a, c) found that the ratio of strain-hardening stiffness to initial stiffness stayed in a relatively fixed range fluctuating between 8% and 12%. A similar situation can be observed in this paper, which can be seen in Table 5. In general, the ratio ranges from 7.3% to 15.6% with a mean value of 10.5% for joints with hollow section columns, while it fluctuates between 6.1% and 18.8% with a mean value of 10.8% for joints with concrete-filled columns. Given that several defect specimens such as I-150 and R160-160, which are too weak and small in size, can be ignored, the strain-hardening stiffness is suggested to be 8% to 10% of the initial stiffness.

As discussed above, the strain-hardening exponents have apparent influences on the moment-rotation curves, especially for the strain-hardening stiffness. This is a unique discrepancy between stainless steel and carbon steel. Therefore, the specific ratios of strain-hardening stiffness to initial stiffness are determined by regression analysis based on 209 models and the fitting expression is indicated in Fig. 22. After key parameters including the initial stiffness, moment capacity and strain-hardening stiffness are determined, the moment-rotation relationship of beam-to-column joints are expected to be obtained for further frame analysis (Liew 2001).

5. Conclusions

The moment-rotation relationship of stainless steel beam-to-column joints with hollow and concrete-filled tubular columns have been investigated by using numerical analysis. The numerical results have been validated with independent experimental results, and extensive parametric studies have been implemented to assess factors that affect structural performance remarkably. A comparison between design codes and FEM results has been discussed and related design recommendations have been proposed. Some main conclusions are herein drawn:

- Finite element model developed is reliable to predict the performance of stainless steel beam-to-column joints in terms of fracture and deformation. Initial geometric imperfections and residual stresses are shown to have little effects on the moment-rotation response of flexural joints.
- Swayed joints with hollow columns can impair the moment resistance significantly compared to braced ones. Concrete filled in columns is able to provide sufficient rigidity, and thus can improve structural performance of swayed joints.
- Strain-hardening exponents have apparent influences on the strain-hardening stiffness resulting in a large fluctuation of moment resistance.
- Some other parameters that affect the joint behaviour considerably include the strength of stainless steel, diameter of bolts, thickness of endplates, position of bolts, section of beams and columns. The axial load ratio on the top of columns is found to have little contributions to the flexural response provided that the load is less than member capacity of columns.
- AS/NZS 2327 provides more accurate predictions of joint behaviour than EN 1993-1-8 in terms of the initial stiffness and moment capacity when tubular columns are used.
- The ratio of strain-hardening stiffness to initial stiffness remains to fluctuate in a small range for the semi-rigid beam-to-column joints and the value is recommended to be 8%-10%. Meanwhile, the specific ratio related to strain-hardening exponents can be determined according to the regression analysis.

Acknowledgments

The research described in this paper is financially supported by the Australian Research Council (ARC) under its Discovery Scheme (Project No: DP180100418). The financial support is gratefully acknowledged. The authors acknowledge the University of Sydney HPC service for providing resources that have contributed to the research results in this paper.

References

ABAQUS (2016), User Manual; Version 6.16, DS SIMULIA Corp, Providence, RI, USA.

Arrayago, I. and Real, E. (2016), "Experimental study on ferritic stainless steel simply supported and continuous beams", *J. Constr. Steel Res.*, **119**, 50-62. https://doi.org/10.1016/j.jcsr.2015.12.006

Arrayago, I., Real, E. and Gardner, L. (2015), "Description of stress–strain curves for stainless steel alloys", *Mater. Des.*, **87**, 540-552. https://doi.org/10.1016/j.matdes.2015.08.001

AS 4100-1998 (1998), Steel structures; Australia.

AS/NZS 2327-2017 (2017), Composite structures—Composite steel-concrete construction in buildings; Australia.

Ashraf, M., Gardner, L. and Nethercot, D.A. (2008), "Structural stainless steel design: Resistance based on deformation capacity", *J. Struct. Eng.*, **134**(3), 402-411. https://doi.org/10.1061/(ASCE)0733-9445(2008)134:3(402)

Averseng, J., Bouchair, A. and Chateauneuf, A. (2017), "Reliability analysis of the nonlinear behaviour of stainless steel cover-plate joints", *Steel Compos. Struct., Int. J.*, **25**(1), 45-55. https://doi.org/10.12989/scs.2017.25.1.045

Baddoo, N.R. (2008), "Stainless steel in construction: A review of research, applications, challenges and opportunities", *J. Constr. Steel Res.*, **64**(11), 1199-1206. https://doi.org/10.1016/j.jcsr.2008.07.011

BS EN 10088-1 (2014), Stainless steels. part 1: list of stainless steels: European Committee for Standardization, Brussels, Belgium.

Cai, Y. and Young B. (2018), "Bearing resistance design of stainless steel bolted connections at ambient and elevated temperatures", *Steel Compos. Struct., Int. J.*, **29**(2), 273-286. https://doi.org/10.12989/scs.2018.29.2.273

Cai, Y. and Young, B. (2019), "Experimental investigation of carbon steel and stainless steel bolted connections at different strain rates", *Steel Compos. Struct., Int. J.*, **30**(6), 551-565. https://doi.org/10.12989/scs.2019.30.6.551

Dai, X. and Lam, D. (2010), "Axial compressive behaviour of stub concrete-filled columns with elliptical stainless steel hollow sections", *Steel Compos. Struct., Int. J.*, **10**(6), 517-539. https://doi.org/10.12989/scs.2010.10.6.517

Elflah, M., Theofanous, M., Dirar, S. and Yuan, H. (2018a), "Behaviour of stainless steel beam-to-column joints—Part 1: Experimental investigation", *J. Constr. Steel Res.*, **152**, 183-193. https://doi.org/10.1016/j.jcsr.2018.02.040

Elflah, M., Theofanous, M. and Dirar, S. (2018b), "Behaviour of stainless steel beam-to-column joints-part 2: Numerical modelling and parametric study", *J. Constr. Steel Res.*, **152**, 194-212. https://doi.org/10.1016/j.jcsr.2018.04.017

Elflah, M., Theofanous, M., Dirar, S. and Yuan, H. (2019), "Structural behaviour of stainless steel beam-to-tubular column joints", *Eng. Struct.*, **184**, 158-175. https://doi.org/10.1016/j.engstruct.2019.01.073

EN 1993-1-1 (2005), Eurocode 4: Design of steel structures. part 1–1: general rules and rules for buildings: European Committee for Standardization, Brussels, Belgium.

EN 1993-1-5 (2006), Eurocode 4: Design of steel structures. part 1–5: plated structural elements: European Committee for Standardization, Brussels, Belgium.

EN 1993-1-8 (2010), Eurocode 4: Design of steel structures. part 1–8: design of joints: European Committee for Standardization, Brussels, Belgium.

EN 1994-1-1 (2004), Eurocode 4: Design of composite steel and concrete structures. part 1–1: general rules and rules for buildings: European Committee for Standardization, Brussels, Belgium.

Gardner, L. and Nethercot, D.A. (2004), "Experiments on stainless steel hollow sections—Part 1: Material and cross-sectional behaviour", *J. Constr. Steel Res.*, **60**(9), 1291-1318. https://doi.org/10.1016/j.jcsr.2003.11.006

Gkantou, M., Kokosis, G., Theofanous, M. and Dirar, S. (2019), "Plastic design of stainless steel continuous beams", *J. Constr. Steel Res.*, **152**, 68-80. https://doi.org/10.1016/j.jcsr.2018.03.025

Han, L.H., Xu, C.Y. and Tao, Z. (2019), "Performance of concrete filled stainless steel tubular (CFSST) columns and joints: Summary of recent research", *J. Constr. Steel Res.*, **152**, 117-131. https://doi.org/10.1016/j.jcsr.2018.02.038

Hasan, M.J., Ashraf, M. and Uy, B. (2017), "Moment-rotation behaviour of top-seat angle bolted connections produced from austenitic stainless steel", *J. Constr. Steel Res.*, **136**, 149-161. https://doi.org/10.1016/j.jcsr.2017.05.014

Huang, Y. and Young, B. (2014), "Experimental investigation of cold-formed lean duplex stainless steel beam-columns", *Thin-Wall. Struct.*, **76**, 105-117. https://doi.org/10.1016/j.tws.2013.11.006

Jandera, M. and Machacek, J. (2014), "Residual stress influence on material properties and column behaviour of stainless steel SHS", *Thin-Wall. Struct.*, **83**, 12-18. https://doi.org/10.1016/j.tws.2014.03.013

Jaspart, J.P. (1991), "Study of the semi-rigidity of beam-to-column joints and its influence on the resistance and stability of steel buildings", Ph.D. Thesis, Liège University, Liège, Belgium.

Kim, T. and Lim, J. (2013), "Ultimate strength of single shear two-bolted connections with austenitic stainless steel", *Int. J. Steel Struct.*, **13**(1), 117-128. https://doi.org/10.1007/s13296-013-1011-z

Kiymaz, G. and Seckin, E. (2014), "Behavior and design of stainless steel tubular member welded end connections", *Steel Compos. Struct., Int. J.*, **17**(3), 253-269. https://doi.org/10.12989/scs.2014.17.3.253

Korol, R.M., Ghobarah, A. and Mourad, S. (1993), "Blind bolting W-shape beams to HSS columns", *J. Struct. Eng.*, **119**(12), 3463-3481. https://doi.org/10.1061/(ASCE)0733-9445(1993)119:12(3463)

Lee, C.H., Chang, K.H., Park, K.T., Shin, H.S. and Lee, M. (2014), "Compressive strength of girth-welded stainless steel circular hollow section members: Stub columns", *J. Constr. Steel Res.*, **92**, 15-24. https://doi.org/10.1016/j.jcsr.2013.09.004

Liew, J.Y.R. (2001), "State-of-the-art of advanced inelastic anaysis of steel and composite structures", *Steel Compos. Struct., Int. J.*, **1**(3), 341-354. https://doi.org/10.12989/scs.2001.1.3.341

Lopes, N., Manuel, M., Sousa, A.R. and Real, P.V. (2019), "Parametric study on austenitic stainless steel beam-columns with hollow sections under fire", *J. Constr. Steel Res.*, **152**, 274-283. https://doi.org/10.1016/j.jcsr.2018.04.018

Lui, W.M., Ashraf, M. and Young, B. (2014), "Tests of cold-formed duplex stainless steel SHS beam–columns", *Eng. Struct.*, **74**, 111-121. https://doi.org/10.1016/j.engstruct.2014.05.009

Mirambell, E. and Real, E. (2000), "On the calculation of deflections in structural stainless steel beams: an experimental and numerical investigation", *J. Constr. Steel Res.*, **54**(1), 109-133. https://doi.org/10.1016/S0143-974X(99)00051-6

Mursi, M. and Uy, B. (2003), "Strength of concrete filled steel box columns incorporating interaction buckling", *J. Struct. Eng.*, **129**(5), 626-639. https://doi.org/10.1061/(ASCE)0733-9445(2003)129:5(626)

Paul, A., Gleich, L.B. and Kahn, L.F. (2017), "Structural Performance of Prestressed Concrete Bridge Piles Using Duplex Stainless Steel Strands", *J. Struct. Eng.*, **143**(7), 04017042. https://doi.org/10.1061/(ASCE)ST.1943-541X.0001770

Pavlović, M., Marković, Z., Veljković, M. and Buđevac, D. (2013), "Bolted shear connectors vs. headed studs behaviour in push-out tests", *J. Constr. Steel Res.*, **88**, 134-149. https://doi.org/10.1016/j.jcsr.2013.05.003

Ramberg, W. and Osgood, W.R. (1943), "Description of stress–strain curves by three parameters", Technical Note No. 902, National Advisory Committee for Aeronautics, Washington DC, USA.

Rasmussen, K.J. (2003), "Full-range stress–strain curves for stainless steel alloys", *J. Constr. Steel Res.*, **59**(1), 47-61. https://doi.org/10.1016/S0143-974X(02)00018-4

Real, E., Arrayago, I., Mirambell, E. and Westeel, R. (2014), "Comparative study of analytical expressions for the modelling of stainless steel behaviour", *Thin-Wall. Struct.*, **83**, 2-11. https://doi.org/10.1016/j.tws.2014.01.026

Shams, M. and Saadeghvaziri, M.A. (1999), "Nonlinear response of concrete-filled steel tubular columns under axial loading", *Struct. J.*, **96**(6), 1009-1017.

Tao, Z., Hassan, M.K., Song, T.Y. and Han, L.H. (2017), "Experimental study on blind bolted connections to concrete-filled stainless steel columns", *J. Constr. Steel Res.*, **128**, 825-838. https://doi.org/10.1016/j.jcsr.2016.10.016

Tokgoz, S. (2015), "Tests on plain and steel fiber concrete-filled stainless steel tubular columns", *J. Constr. Steel Res.*, **114**, 129-135. https://doi.org/10.1016/j.jcsr.2015.07.013

Tondini, N., Rossi, B. and Franssen, J.M. (2013), "Experimental investigation on ferritic stainless steel columns in fire", *Fire Safety J.*, **62**, 238-248. https://doi.org/10.1016/j.firesaf.2013.09.026

Wang, J.F. and Chen, L. (2012), "Experimental investigation of extended end plate joints to concrete-filled steel tubular columns", *J. Constr. Steel Res.*, **79**, 56-70. https://doi.org/10.1016/j.jcsr.2012.07.016

Wang, J., Uy, B. and Li, D.X. (2018a), "Analysis of demountable steel and composite frames with semi-rigid bolted joints", *Steel Compos. Struct., Int. J.*, **28**(3), 363-380. https://doi.org/10.12989/scs.2018.28.3.363

Wang, J., Uy, B., Thai, H.T. and Li, D.X. (2018b), "Behaviour and design of demountable beam-to-column composite bolted joints with extended end-plates", *J. Constr. Steel Res.*, **144**, 221-235. https://doi.org/10.1016/j.jcsr.2018.02.002

Wang, J., Zhu, H., Uy, B., Patel, V., Aslani, F. and Li, D.X. (2018c), "Moment-rotation relationship of hollow-section beam-to-column steel joints with extended end-plates", *Steel Compos. Struct., Int. J.*, **29**(6), 717-734. http://dx.doi.org/10.12989/scs.2018.29.6.717

Yousuf, M., Uy, B., Tao, Z., Remennikov, A. and Liew, J.R. (2014), "Impact behaviour of pre-compressed hollow and concrete filled mild and stainless steel columns", *J. Constr. Steel Res.*, **96**, 54-68. https://doi.org/10.1016/j.jcsr.2013.12.009

Yuan, H.X., Wang, Y.Q., Shi, Y.J. and Gardner, L. (2014), "Residual stress distributions in welded stainless steel sections", *Thin-Wall. Struct.*, **79**, 38-51. https://doi.org/10.1016/j.tws.2014.01.022

Zhao, O., Gardner, L. and Young, B. (2016), "Experimental study of ferritic stainless steel tubular beam-column members subjected to unequal end moments", *J. Struct. Eng.*, **142**(11), 04016091. https://doi.org/10.1061/(ASCE)ST.1943-541X.0001563

DL